Seasonal variation of methane microseepage in the Dawanqi oilfield (China): a possible climatic control

Yujia Zhao[1], Guojian Wang[2], Giuseppe Etiope[3,4], Yong wang[5], Zhenzhen Zhu[1], Chunhui Wang[1], Xufeng, Chen[1], Junhong Tang[1]

[1]College of Materials Science and Environmental Engineering, Hangzhou Dianzi University, Hangzhou, China

[2]Wuxi Research Institute of Petroleum Geology, Research Institute of Petroleum Exploration and Production, SINOPEC, Wuxi, China

[3]Istituto Nazionale di Geofisica e Vulcanologia, Rome, Italy

[4]Faculty of Environmental Science and Engineering, Babes-Bolyai University, Cluj-Napoca, Romania

[5]Department of Kela Oil and Gas Development, PetroChina Tarim Oilfield Company, Korla, Xinjiang, China

Corresponding author: Junhong Tang (tang_jhjh@163.com)

†College of Materials Science and Environmental Engineering, Hangzhou Dianzi University, Hangzhou, China

Key Points:

- Microseepage of thermogenic gas over the Dawanqi oilfield is confirmed by molecular and isotopic hydrocarbon data in 4-m deep boreholes.
- Contrarily to previous observations in other petroleum basins, methane fluxes to the atmosphere are higher in summer and lower in winter due to relevant ice thickness in the soil.
- Methanotrophic consumption and the ice-snow barrier effect compete in the establishment of the seasonal microseepage pattern; microseepage may increase in future milder winters due to regional climatic warming.

Abstract

Natural gas microseepage in petroleum-bearing sedimentary basins is an important complement to geophysical methods in oil-gas exploration and a natural source of methane (CH_4) for the atmosphere. Microseepage, typically occurring in correspondence with petroleum fields throughout the world, is generally lower in summer, due to temperature-driven methanotrophic consumption, and higher in winter. The global estimates of microseepage methane emission have, however, relatively high uncertainties because of limited amounts of flux data, leading to poor knowledge of the spatial distribution and temporal variability of the gas emission factors. We studied the seasonal variation of microseepage flux to the atmosphere from a petroleum field in China (the Dawanqi oilfield), through methane flux measurements performed in summer 2014, winter 2015 and summer 2019. Winter data refer to frozen soil conditions, with snow cover and ice thickness in the soil exceeding 60 cm. Gas concentration (CH_4, CO_2, C_{2+} alkanes) and stable C isotopic composition of CH_4 and CO_2 in shallow (4 m deep) boreholes confirmed the existence of thermogenic gas seepage. Methane microseepage is higher in summer and lower or nil in winter. This seasonal trend is opposite to what was observed in areas where winter soil is not or poorly frozen. Our data suggest that seasonal microseepage variation may not be univocal worldwide, being strongly dependent on the presence of ice and snow cover in winter. The regional increase of temperature due to climate change, already demonstrated for the Tarim Basin over the last 50 years, could, in the future, reduce winter ice and enhance annual methane emission to the atmosphere.

Keywords: Microseepage, methane, petroleum fields, seasonal variations, iced soil

1 Introduction

Microseepage of methane (CH_4) on the Earth's surface is an important geochemical proxy of subsurface petroleum reservoirs and source rocks (Price, 1986; Klusman & Saaed, 1996; Saunders et al., 1999; Brown, 2000; Kvenvolden & Rogers, 2005; Xiao et al., 2019) and a natural source of methane for the atmosphere (Etiope et al., 2009; Etiope & Klusman, 2010; Etiope, 2015; Tang et al., 2017; Etiope & Schwietzke, 2019). Microseepage is likely the most important geological source of methane, globally estimated to be in the order of 10-24 Tg yr^{-1}, followed by macro-seepage emissions such as mud volcanoes, gas-oil seeps and submarine seeps (Etiope & Klusman, 2010; Etiope et al., 2019; Etiope & Schwietzke, 2019). Many studies show that (a) hydrocarbon microseepage dominantly occurs in correspondence with petroleum fields (mostly gas fields), and in particular along the faulted boundaries of the reservoirs (Macgregor, 1993; Ciotoli et al., 2020), and (b) that the gas flux to the atmosphere is higher in winter and lower in summer, in relation to temperature-driven methanotrophic consumption (Klusman, 2003; Etiope & Klusman, 2010). Methane flux data are however available only from a few petroleum provinces (mostly in central United States, Italy, Romania and China) and their seasonal variation is scarcely known. The actual global area of microseepage is, then, only theoretically predictable and the emission factors, which are essential for bottom-up emission estimates, have relatively high uncertainty (Etiope & Schwietzke, 2019; Saunois et al., 2020). In particular, there are no sufficient data showing the effect of ice content in the soil in winter. Although methanotrophic consumption is lower in winter, leading to enhanced methane release to the atmosphere, in some regions the presence of ice may reduce the gas exhalation (as observed in permafrost regions; e.g., O'Connor et al., 2010), inverting the seasonal trend.

The oil field of Dawanqi, in the Tarim Basin (China), offered the possibility to investigate the seasonal changes of microseepage in conditions of highly frozen soil, as in typical extreme desert climates: the Tarim Basin has January mean temperatures of -10 to -20 °C (Chen et al., 2007). Microseepage in the summer season (summer 2014) in the Dawanqi area was already investigated by Tang et al. (2017). Seepage was found to be strictly correlated with faults and with the occurrence of subsurface gas-oil pools related to the Dawanqi petroleum system (Tang et al., 2017).

In this work, we show new microseepage flux data acquired in winter 2015 and summer 2019, along the same transects investigated in 2014. Winter data refer to frozen soil conditions, with snow cover and ice thickness in the soil exceeding 60 cm. The concentration of methane, heavier alkanes (ethane, propane, butane, and pentane) and carbon dioxide (CO_2) in the ground, and the stable C isotopic compositions of CH_4 and CO_2 in summer, at depths down to about 4 m, were also analyzed to assess the microseepage mechanism. The Tarim Basin is experiencing regional warming related to climate change (mean annual temperature increased of about 1 °C over the past 50 years; Chen et al., 2007), and our multi-seasonal study can predict the effect of this warming on methane microseepage in future milder winters.

2 Environmental and geological setting of the Dawanqi oilfield

The Dawanqi oilfield is located in the western part of the Kuqa-Baicheng depression, Tarim Basin (Figure 1). The region is characterized by an arid climate, low land productivity and severe soil salinization, resulting in rare vegetation and no biological methanogenic production near the surface. The dry soil, type "Gobi" (Luo et al., 2014), is generally a net sink of atmospheric methane. The average annual temperature is 10.6-11.5 °C; monthly mean temperature ranges from 20 to 30 °C in July and -10 to -20 °C in January (Chen et al., 2007). The snow cover, averagely lasts from 71 to 120 days and is homogeneously distributed with a thickness of 10-15 cm (Ding et al., 2018). The frozen soil reaches depths of about 90 cm (Fu et al., 2013; Hu et al., 2014). In the winter 2015, we observed ice thickness in the soil exceeding 60 cm; the temperature ranged from -14 °C to -10 °C and the atmospheric pressure was 8.96×10^4 - 9×10^4 Pa.

Discontinuous aquifers occur at a depth > 4.2 m. The geology of the Dawanqi oilfield was described in detail in previous papers (e.g., Tang et al., 2017). Here, we highlight that the area is highly faulted and fractured (dominated by the Tuzimazha fault system), hydrocarbon reservoirs are relatively shallow (170 to 700 m) in Quaternary to Neogene sandstones, while oil and gas are generated in Triassic and Jurassic coal-bearing formations (Zhao et al., 2003; Kuang et al., 2003; Kuang & Jin, 2005; Yang et al., 2006). Gas reservoirs have at least 89 vol% of thermogenic CH_4 ($\delta^{13}C$: -18 to -38 ‰ VPDB), with C_{2+} alkanes (~8 vol%), N_2 (2 vol%) and CO_2 (0.5 vol%) (Wang et al., 2012).

3 Methods

3.1 Field work

3.1.1 Ground gas sampling

Ten locations were selected for installation of tubing for nested soil gas sampling, nine in the proximity of fault systems or in correspondence with reservoirs, and one in a control area, outside the petroleum field. Sampling tubes were installed at depths of 0.3, 0.6, 0.9, 1.2, 1.5, 1.8, 2.1, 2.4, 2.7 m, 3 m (some at 3.5 m and 4 m; Fig. 2a). Groundwater was encountered at 4.2 m at some locations, and in these cases gas samples were preferably collected at maximum 3 m. The sampling layer was composed of sand and were sealed using bentonite, preventing gas exchange at different depths. High density polyethylene tubing (0.64 cm OD, 0.32 cm ID) was inserted in each sampling layer (Fig. 2b). The polyethylene tubing was closed at the top with a rubber pad, which is wrapped with vacuum sealant tape at the junction of the gas sampling tube. This arrangement allows sampling with a syringe. Ground gas was purged from the probe using a syringe after 10 days. Then the gas samples were drawn and injected into a 500 ml glass vial filled with saturated brine. In total, 116 gas samples were collected in summer 2016 and 2019, and sent to the laboratory for molecular and stable C composition (CH_4, CO_2) analyses.

3.1.2 Microseepage methane flux measurements

For this work we used data of methane flux measurements performed in August 2014 (51 points), along three transects (MT1, MT2 and MT3) crossing the main reservoirs and faults (data published in Tang et al. 2017) and carried out new measurements, along the same transects in January 2015 (42 points) and August 2019 (31 points), as illustrated in Fig 3. In January 2015 the investigated area was homogeneously covered by snow (about 10-15 cm thick). As in 2014, 2015 and 2019 CH_4 flux measurements were performed using a portable laser-based gas analyzer (LGR915-0011; detection limit of 5 ppbv CH_4, 1σ precision of 0.6 ppbv) combined with a closed accumulation chamber (radius of 37 cm and height of 12 cm; Fig. 3).

The chamber was inserted into the soil to a depth of about 5 cm, so that internal net volume was 3×10^4 cm^3 (during winter measurements the snow cover inside the chamber was removed). Gas Flux was then calculated by using a linear regression of gas concentration buildup in the chamber, as typically performed for closed chambers. Each measurement was based on gas accumulation times of about 20 min. Methodological and calculation details, and further references, are reported in Tang et al. (2007) and Tang et al. (2017). Sampling interval along each transect varied from 50 to 300 m, depending on the availability of suitable ground conditions for installation of the closed chamber. As a control and for comparison, measurements were also taken in an area located outside the petroleum field, approximately 50 km from the field boundary.

3.2 Laboratory analyses

The concentrations of methane, ethane, propane, n-butane, i-butane, n-pentane, i-pentane and CO_2 in the gas samples were analyzed by Perkin-Elmer model Auto system XL（FID/TCD） gas chromatograph with flame ionization detection, which was calibrated by using standards of 2.04 ppmv CH_4, 1.01 ppmv C_2H_6, 1.05 ppmv C_3H_9 (provided by Dalian Special Gases Corporation Limited, China) before and after each batch of measurements. The chromatograph used alumina column (Al_2O_3 PLOT, 50m×0.53mm) and operated isothermally at 120 °C; N_2 was the carrier gas (flow of 30 mL/min); the FID detector operated at 180 °C. The values of hydrocarbons were determined with a precision of 0.01 ppmv.

The stable C isotopic composition of CH_4 and CO_2 were determined by gas chromatography-mass spectrometry, based on MAT-253 isotope mass spectrometer by Thermo Finnigan. The GC used a Porapak QCP7551 capillary column (27.5m×0.32mm×10 m) and He as carrier gas (flow of 1.8 mL/min). CH_4 is oxidised to CO_2 in combustion furnace and the isotopic composition of the CO_2 is analysed by isotope-ratio mass spectrometry. The $\delta^{13}C$ values were determined with a precision of 0.4‰ (*n*=10). Chinese national carbonate standard GBW04405 with known isotopic values was used for isotope calibration. The stable C isotopic compositions are reported using notation per mill (‰) relative to VPDB (Vienna Pee Dee Belemnite).

4 Results

4.1. Gas concentration profiles in the ground

CH_4 concentration in the ground (Fig. 5) increases with depth, in all sites located within the petroleum field, from near atmospheric values at 0.3 m, to more than 30,000 ppmv at the depth of 3 m (profile 545-13; Fig. 5). The control site, outside the field, did not provide any significant gas increase with depth, with CH_4 always around 2 ppmv. Within the petroleum field area, $\delta^{13}C$-

CH_4 increased from values near the atmospheric level (-44 to -46 ‰) at 0.3 m, to values around -20 ‰ below 1.5 m. From 1 to 4 m, the CH_4 isotopic composition is quite stable ($\delta^{13}C$ within -20 and -30 ‰), but it decreases progressively and rapidly towards the surface.

The C_1/C_{2+} ratio (Fig. 6) also increases with depth, which implies progressive, relative decrease of CH_4 towards the surface (as shown in Figure 5). C_{2+} gases are higher (see Table S2 in Supporting Information) at the 545-13 site (at the fault intersection), where also CH_4 is higher.

CO_2 concentration also increases with depth, up to 10,100 ppmv, although with wider oscillations (Fig. 7). Its stable C isotope composition does not change significantly below 1 m, with $\delta^{13}C$-CO_2 values around -16 to -22 ‰, and increases reaching the atmospheric value (about -9 ‰) near the surface. A slight, less pronounced CO_2 increase (up to 2000 ppmv) is observed also in the control site.

Overall, the hydrocarbon data confirm the existence of thermogenic gas seepage from depth, as recorded in the oil-gas migration literature (Zhang et al., 1998; Hou & Su, 2001). The seeping gas has however higher $C_1/(C_2+C_3)$ ratio compared to reservoir (Fig. 8): this is typical of gas seepage and is generally interpreted as due to molecular segregation during upward migration (Etiope et al. 2009). The increase of CO_2 with depth could, partially, be also due to gas seepage, as the Dawanqi reservoirs host 0.5 vol.% CO_2. Additional CO_2 may derive from aquifer degassing (including CH_4 oxidation).

The data at the shallower depths (< 1 m) suggest contamination of atmospheric air. This could be due to air leakage in the shallowest tubing, a less effective removal of air from the pipes before sampling, or flow of air into the soil due to atmospheric pumping, typically induced by barometric pressure and wind changes (e.g., Wyatt et al. 1995).

4.2 Methane flux

Methane microseepage flux was measured along the three transects MT1, MT2 and MT3, both in January 2015 and August 2019, confirming the seepage potential of the area studied in August 2014 and discussed in Tang et al. (2017). Descriptive statistics of the flux data are summarized in Table 1 and the individual values along the three transects are shown in Figures 9, 10 and 11 (all data are available in the Supporting Information Table S1). The data clearly show that summer fluxes (both in 2014 and 2019) are systematically higher than the winter ones. Fig. 12 shows the microseepage CH_4 histogram distribution in the two seasons. The methane flux in summer (median value 0.49 mg m^{-2} d^{-1}; mean value 13.87 mg m^{-2} d^{-1}, including both 2014 and 2019 data) is mostly distributed between 0 and 5 mg m^{-2} d^{-1}, which is consistent with the global pattern of microseepage values (Etiope & Klusman, 2010). Summer fluxes reach orders of 10^2 mg m^{-2} d^{-1}, and positive are in 76.8 % of the cases. The highest values were observed near major faults (the highest value of 329.9 mg m^{-2} d^{-1} at point 554-11 is located over the intersection of two faults). Winter fluxes are mostly negative (81.4 % of the January 2015 cases), and not exceeding 0.53 mg m^{-2} d^{-1}. Where the measurements were taken exactly at the same point (42 cases), the summer-winter difference ranges from -1.41 to 329.9 mg m^{-2} d^{-1} (vertical lines in Figs. 9 to 11).

5 Discussion and conclusions

The ground gas profiles clearly demonstrated the existence of thermogenic gas seepage in correspondence with the Dawanqi oilfield. The seepage is higher in the proximity of the fault systems, consistent with numerous seepage studies and models (Etiope, 2015; Ciotoli et al., 2020). The profiles from 4 m to 1 m, characterized by the absence of significant CH_4 isotopic fractionation compared to reservoir gas, suggest that seepage is likely driven by advective process (gas migration driven by pressure gradients), as considered in the crustal degassing literature (Etiope & Martinelli, 2002; Etiope, 2015). The $\delta^{13}C$-CH_4 values at depth >1.5 m are consistent with those measured in the deeper Neogene reservoirs (Tang et al., 2017). Near the surface, however, $\delta^{13}C$-CH_4 and $\delta^{13}C$-CO_2 may slightly increase and decrease, respectively, due to methanotrophic oxidation (Whiticar & Faber, 1986; Phelps et al., 1989; Benstead & King, 1997). The $\delta^{13}C$-CH_4 values at the soil-atmosphere interface (i.e. the isotopic value of methane actually entering the atmosphere and measured within the chamber) was reported in Tang et al., (2017): methane accumulating in the chamber is generally more enriched in ^{13}C than atmospheric air, with $\delta^{13}C$-CH_4 values (measured in 17 points) ranging from -46.3 ‰ to -30.7 ‰; the values increase with the flux, reflecting the input and dilution in the chamber of the thermogenic gas from the reservoir ($\delta^{13}C$: -18 to -38 ‰ VPDB; Fig.8) with atmospheric air ($\delta^{13}C$~ -47 ‰ VPDB).

The gas microseepage flux is then controlled by near-surface soil conditions, which change seasonally. The fluxes are higher in summer and lower in winter. This trend is opposite to the one typically observed in areas with less extreme climatic conditions. It is generally considered, in fact, that microseepage is lower in summer, compared to winter, because of the higher methanotrophic consumption (Klusman et al., 2000; Etiope & Klusman, 2010). However, Klusman, (2003) reported variable patterns over a petroleum field in Colorado (Rangely): the fluxes in the winter 2001/2002 were higher than in summer 2001 (as expected because of the methanotrophic consumption variability), but the fluxes in winter 2000/2001 were lower than those in summer 2001. This suggests that not all winters lead to higher microseepage. A similar winter seepage decrease is observed at the Dawanqi oilfield. The Dawanqi area is characterized by extreme climatic conditions in winter, with abundant snow covers (about 10-15 cm of snow were observed in our winter measurements in 2015) and significant ice thickness in the soil (reaching depths of about 90 cm; Fu et al., 2013; Hu et al., 2014). The higher winter fluxes reported by Klusman, (2003) were actually reported in less cold climatic conditions, with reduced presence of snow and ice (thickness not exceeding 60 cm; Klusman, 2003). It is likely, then, that significant ice thickness and snow cover act as a barrier for microseepage, and this effect prevails on the one (in opposite direction) of the lower methanotrophic consumption (Wu et al., 2014). Methanotrophic consumption seems to occurs also in presence of snow and ice, as also observed by Klusman (2003). We also note that the methane fluxes in summer (Figs. 9-11) are consistent with the order of magnitude of the local theoretical microseepage derived by a global gridding, process-based and statistical, model (Etiope et al., 2019): the microseepage grid cells in correspondence with the Dawanqi oilfield have mostly theoretical (modeled) fluxes in the range of 0.01–12 mg m^{-2} d^{-1}.

Overall, our data suggest that seasonal variations of microseepage are not the same everywhere, as they depend on the specific winter climate conditions: the lower methanotrophic consumption (leading to higher fluxes) and the ice-snow barrier effect (leading to lower fluxes) seem to compete in the establishment of the seasonal pattern. This pattern is expected to be "normal" (mostly controlled by methanotrophic activity) in temperate and not extreme winter climatic regions, and "inverse" in extremely cold regions, as the Dawanqi region.

The Tarim Basin is experiencing climatic warming, as observed over the last 50 years, with an average temperature increase of 1 °C (Chen et al., 2007). This implies that, if warming will continue in the future, winters may become milder and the presence of ice in the soil may decrease. If so, it is expected that winter methane seepage will tend to increase, in a process similar to that observed in permafrost and sub-arctic regions (Anisimov & Reneva, 2006;

O'Connor et al., 2010b; Masyagina & Menyailo, 2020; Anthony et al., 2020). Further microseepage measurements in the Dawanqi area shall be performed in the next winters to monitor and confirm the possible climate control of microseepage methane exhalations. A more careful investigation, including modeling, on microseepage mechanisms (advection vs diffusion) and methane oxidation in iced and ice-free soil, will be essential to improve process-based models for global emission estimates.

Acknowledgments

This work was supported by the Joint Funds of the National Natural Science Foundation of China (grants U2003101) and National Natural Science Foundation of China (grants 41872126 and 41373121). Thanks to Mr. Suo Xiaodong (Bureau of Geophysical Prospecting INC., China National Petroleum Corporation) for his guidance on petroleum geology of the Dawanqi field.

References

Anisimov, O., & Reneva, S. (2006). Permafrost and Changing Climate: The Russian Perspective. *AMBIO: A Journal of the Human Environment*, *35*(4), 169–175. https://doi.org/10.1579/0044-7447(2006)35[169:PACCTR]2.0.CO;2

Anthony, K., Lindgren, P., Hanke, P., Engram, M., Anthony, P., Daanen, R., et al. (2020). Decadal-scale hotspot methane ebullition within lakes following abrupt permafrost thaw. *Environmental Research Letters*. https://doi.org/10.1088/1748-9326/abc848

Benstead, J., & King, G. (1997). Response of methanotrophic activity in forest soil to methane availability. *FEMS Microbiology Ecology*, *23*(4), 333–340. https://doi.org/10.1111/j.1574-6941.1997.tb00414.x

Brown, A. (2000). Evaluation of Possible Gas Microseepage Mechanisms. *AAPG Bulletin*, *84*(11), 1775–1789. https://doi.org/10.1306/8626C389-173B-11D7-8645000102C1865D

Chen, Y., Li, W., Xu, C., & Hao, X. (2007). Effects of climate change on water resources in Tarim River Basin, Northwest China. *Journal of Environmental Sciences*, *19*(4), 488–493. https://doi.org/10.1016/S1001-0742(07)60082-5

Ciotoli, G., Procesi, M., Etiope, G., Fracassi, U., & Ventura, G. (2020). Influence of tectonics on global scale distribution of geological methane emissions. *Nature Communications*, *11*(1), 2305. https://doi.org/10.1038/s41467-020-16229-1

Ding, Y., Li, Y., Li, L., Yao, N., Hu, W., & Yang, D. (2018). Spatiotemporal variations of snow characteristics in Xinjiang, China over 1961–2013 | Request PDF. *Nordic Hydrology*, *49*(5–6), 1578–1593. https://doi.org/10.2166/nh.2017.035

Etiope, G. (2015). *Natural Gas Seepage: The Earth's Hydrocarbon Degassing*. Springer, Switzerland. https://doi.org/10.1007/978-3-319-14601-0

Etiope, G., & Klusman, R. W. (2010). Microseepage in drylands: Flux and implications in the global atmospheric source/sink budget of methane. *Global and Planetary Change*, *72*(4), 265–274. https://doi.org/10.1016/j.gloplacha.2010.01.002

Etiope, G., & Martinelli, G. (2002). Migration of carrier and trace gases in the geosphere: an overview. *Physics of the Earth and Planetary Interiors*, *129*(3), 185–204. https://doi.org/10.1016/S0031-9201(01)00292-8

Etiope, G., & Schwietzke, S. (2019). Global geological methane emissions: An update of top-down and bottom-up estimates. *Elementa-Science of the Anthropocene*, *7*, 1–9. https://doi.org/10.1525/elementa.383

Etiope, G., Ciotoli, G., Schwietzke, S., & Schoell, M. (2019). Gridded maps of geological methane emissions and their isotopic signature. *Earth System Science Data*, *11*(1), 1–22. https://doi.org/10.5194/essd-11-1-2019

Etiope, G, Feyzullayev, A., & Baciu, C. L. (2009). Terrestrial methane seeps and mud volcanoes: A global perspective of gas origin. *Marine and Petroleum Geology*, *26*(3), 333–344. https://doi.org/10.1016/j.marpetgeo.2008.03.001

Fu, C., Dan, L., Wu, J., & Wei, R. (2013). Variation and Abrupt Change of Maximum Depth of Frozen Soil over Xinjiang Under the Background of Global Warming, 1961-2005. *Journal of Glaciology and Geocryology*, *35*(06), 1410–1418.

Hou, W., & Su, J. (2001). The evidence and characteristics of vertical micro-migration of upper pool's hydrocarbons in northern Tarim Basin (in Chinese). *Xinjiang Petroleum Geology*, (06), 465-468+452–453.

Hu, L., Wu, P., Liang, C., & Zhang, W. (2014). Analyzing the effect of snow cover in spring and winter and air temperature on frozen ground depth in Xinjiang. *Glaciology and Geocryology*, *36*(01), 48–54.

Klusman, R. W. (2003). Rate measurements and detection of gas microseepage to the atmosphere from an enhanced oil recovery/sequestration project, Rangely, Colorado, USA. *Applied Geochemistry*, *18*(12), 1825–1838. https://doi.org/10.1016/s0883-2927(03)00108-2

Klusman, R. W., & Saaed, M. A. (1996). Comparison of Light Hydrocarbon Microseepage Mechanisms, 157–168.

Klusman, R. W., Leopold, M. E., & LeRoy, M. P. (2000). Seasonal variation in methane fluxes from sedimentary basins to the atmosphere: Results from chamber measurements and modeling of transport from deep sources. *Journal of Geophysical Research: Atmospheres*, *105*(D20), 24661–24670. https://doi.org/10.1029/2000JD900407

Kuang, H., & Jin, G. (2005). Reservoir characteristic and evalution of the Kangcun formation in the Dawanqi oilfield Tarim Basin (in Chinese). *Geomechanics*, (01), 81–89.

Kuang, H., Niu, S., & Chen, X. (2003). The diagenetic characteristics and its controlling factors of the Kangcun formation in the Dawanqi oilfield, the Tarim Basin (in Chinese). *Geoscience*, *17*(02), 211–216.

Kvenvolden, K. A., & Rogers, B. W. (2005). Gaia's breath—global methane exhalations. *Marine and Petroleum Geology*, *22*(4), 579–590. https://doi.org/10.1016/j.marpetgeo.2004.08.004

Luo, W., Dong, Z., Qian, G., Feng, M., Lu, J., Wang, M., et al. (2014). Geochemical compositions of surface sediment from Gobi Desert in northern China and its sedimentary significance (in Chinese). *Journal of Desert Research*, *34*(06), 1441–1453.

Macgregor, D. S. (1993). Relationships between seepage, tectonics and subsurface petroleum reserves. *Marine and Petroleum Geology*, *10*(6), 606–619. https://doi.org/10.1016/0264-8172(93)90063-X

Masyagina, O. V., & Menyailo, O. V. (2020). The impact of permafrost on carbon dioxide and methane fluxes in Siberia: A meta-analysis. *Environmental Research*, *182*, 109096. https://doi.org/10.1016/j.envres.2019.109096

Milkov, A. V., & Etiope, G. (2018). Revised genetic diagrams for natural gases based on a global dataset of >20,000 samples. *Organic Geochemistry*, *125*, 109–120. https://doi.org/10.1016/j.orggeochem.2018.09.002

O'Connor, F. M., Boucher, O., Gedney, N., Jones, C. D., Folberth, G. A., Coppell, R., et al. (2010a). Possible role of wetlands, permafrost, and methane hydrates in the methane cycle under future climate change: A review. *Reviews of Geophysics*, *48*(4). https://doi.org/10.1029/2010RG000326

Phelps, T. J., Raione, E. G., White, D. C., & Fliermans, C. B. (1989). Microbial activities in deep subsurface environments. *Geomicrobiology Journal*, *7*(1–2), 79–91. https://doi.org/10.1080/01490458909377851

Price, L. C. (1986). A critical overview and proposed working model of surface geochemical exploration. *Unconventional Methods in Exploration for Petroleum and Natural Gas IV*, 245–309.

Rusticucci, M., Brönnimann, S., Charabi, Y., Dentener, F., Easterling, D., Soden, B., et al. (2014). IPCC (2013), Climate Change 2013, in The Physical Science Basis, Working Group I Contribution to the Fifth Assessment Report of the Intergovernmental Panel on Climate Change, WMO/UNEP, Cambridge (pp. 159–254).

Saunders, D. F., Burson, K. R., & Thompson, C. K. (1999). Model for Hydrocarbon Microseepage and Related Near-Surface Alterations. *AAPG Bulletin*, *83*(1), 170–185. https://doi.org/10.1306/00AA9A34-1730-11D7-8645000102C1865D

Saunois, M., Stavert, A. R., Poulter, B., Bousquet, P., Canadell, J. G., Jackson, R. B., et al. (2020). The Global Methane Budget 2000–2017. *Earth System Science Data*, *12*(3), 1561–1623. https://doi.org/10.5194/essd-12-1561-2020

Tang, J., Bao, Z., Xiang, W., & Gou, Q. (2007). Daily Variation of Natural Emission of Methane to the Atmosphere and Source Identification in the Luntai Fault Region of the Yakela Condensed Oil/Gas Field in the Tarim

Basin, Xinjiang, China. *Acta Geologica Sinica - English Edition*, *81*(5), 771–778. https://doi.org/10.1111/j.1755-6724.2007.tb01001.x

Tang, J., Xu, Y., Wang, G. J., Etiope, G., Han, W., Yao, Z., & Huang, J. (2017). Microseepage of methane to the atmosphere from the Dawanqi oil-gas field, Tarim Basin, China. *Journal of Geophysical Research-Atmospheres*, *122*(8), 4353–4363. https://doi.org/10.1002/2016jd026385

Wang, Q., Bao, J., Xie, Z., & Wang, S. (2012). Geochemical characteristics and genesis of natural gas in the Dawanqi oilfield (in Chinese). *Journal of Yangtze University(Natural Science Edition)*, *9*(08), 28–31.

Whiticar, M. J., & Faber, E. (1986). Methane oxidation in sediment and water column environments—Isotope evidence. *Organic Geochemistry*, *10*(4), 759–768. https://doi.org/10.1016/S0146-6380(86)80013-4

Wu, X., Brueggemann, N., Butterbach-Bahl, K., Fu, B., & Liu, G. (2014). Snow cover and soil moisture controls of freeze-thaw-related soil gas fluxes from a typical semi-arid grassland soil: a laboratory experiment. *Biology and Fertility of Soils*, *50*(2), 295–306. https://doi.org/10.1007/s00374-013-0853-z

Wyatt, J. M., & Knowles, C. J. (1995). Microbial degradation of acrylonitrile waste effluents: the degradation of effluents and condensates from the manufacture of acrylonitrile. *International Biodeterioration & Biodegradation*, *35*(1), 227–248. https://doi.org/10.1016/0964-8305(95)00031-Y

Xiao, C., Wu, X., Wang, D., & Zhu, Y. (2019). Oil-gas information extraction and prospective area prediction based on hydrocarbon microseepage theory: A case study of Salamat Basin in Central Africa (in Chinese). *Remote Sensing for Land & Resources*, *31*(04), 120–127.

Yang, X., Che, C., Yang, S., & Zhao, D. (2006). Reservoir types and distribution regularities in the Dawanqi oilfield (in Chinese). *West China Petrol. Geosci*, (01), 41–44.

Zhang, B., Zhu, H., & Wang, R. (1998). Vertical micro-migration characteristics of deep hydrocarbon gas in the north part of Tarim Basin (in Chinese). *Natural Gas Industry*, (01), 39-42+7–8.

Zhao, M., Song, Y., Liu, S., & Qin, S. (2003). The diffusion influence on gas pool: Dawanqi oilfield as an example (in Chinese). *Natural Gas Geoscience*, (05), 393–397.

Figure captions

Figure 1. Location of Dawanqi oilfield. The main tectonic units and fault systems of the Kuqa depression (northern sector of Tarim Basin) are shown (redrawn from Tang et al. 2017). The dashed lines are the isolines (m) for the top of the Baicheng Sag structure.

Figure 2. Sketch of gas sampling tubes in the ground (a); installation of tubes in a borehole (b).

Figure 3. Gas flux measurements using the closed-chamber method with portable gas analyzer, in summer (a) and winter (b).

Figure 4. Gas flux measurement locations at the Dawanqi oilfield. MT1, MT2 and MT3 are the measurements transects (see also Table S1). Red lines are fault and fracture systems identified by geophysical prospections (see Tang et al. 2017). Stars are the boreholes for ground gas profile. Grey circles are oil wells. Triangles (August 2014), diamonds (January 2015) and squares (August 2019) are the measurement sites of each measurement campaign.

Figure 5. Methane concentration (a) and stable C isotope composition (b) profiles versus depth, in the 4-meter boreholes. All measurements were taken in summer season.

Figure 6. C_1/C_{2+} profiles in the 4-meter boreholes. All measurements were taken in summer season.

Figure 7. CO_2 concentration (a) and stable C isotope composition (b) profiles in the 4-meter holes. All measurements were taken in summer season.

Figure 8. $\delta^{13}C\text{-}CH_4$ vs $C_1/(C_2+C_3)$ diagram for gas samples collected in six ground boreholes, compared to Dawanqi oil-gas reservoir (reservoir data after Wang et al., 2012). CR: CO_2 reduction, F: methyl-type fermentation, SM: Secondary microbial, LMT: late mature thermogenic gas, OA: oil-associated thermogenic gas. Genetic zonation after Milkov & Etiope (2018).

Figure 9. Methane microseepage flux data along transect MT1. Vertical lines highlight the flux difference between summer and winter where measurements were performed at the same point.

Figure 10. Methane microseepage flux data along transect MT2. Vertical lines as in Fig. 5.

Figure 11. Methane microseepage flux data along transect MT3. Vertical lines as in Fig. 5.

Figure 12. Histogram of microseepage flux data in summer (a) and winter (b)

Table caption

Table 1. Descriptive statistics of CH_4 microseepage flux (mg m^{-2} d^{-1})

Table 1 Descriptive statistics of CH_4 microseepage flux (mg m^{-2} d^{-1})

Flux (mg·m^{-2}·d^{-1})		
Parameter	**summer**	**winter**
Mean	13.87	-0.24
Median	0.49	-0.28
Min	-1.41	-1.05
Max	329.9	0.53
Std.dev	50.94	0.33

Figure 1.

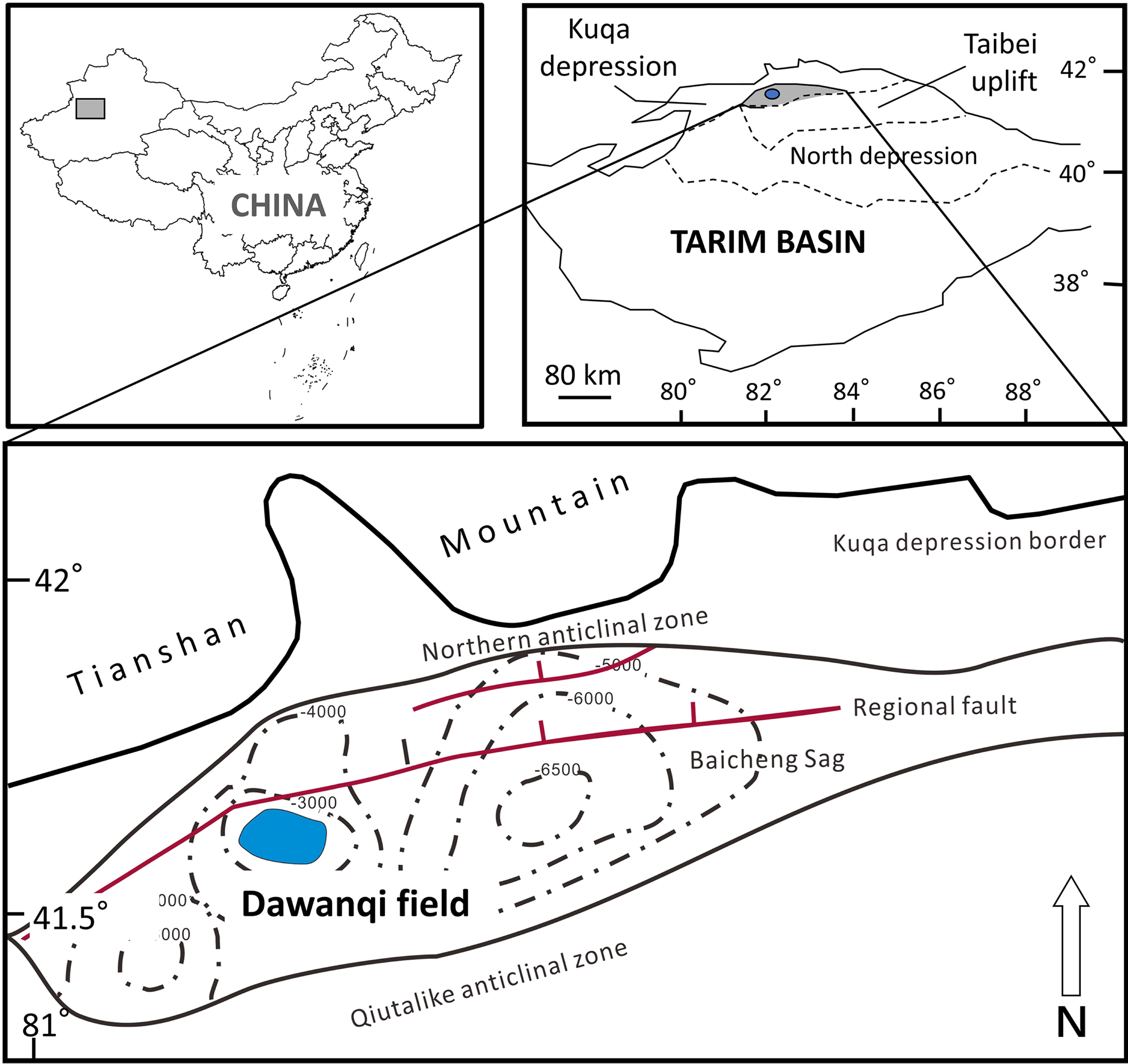

CHINA
Kuqa depression
Taibei uplift
North depression
TARIM BASIN
80 km
80°
82°
84°
86°
88°
42°
40°
38°
Mountain
Tianshan
Kuqa depression border
Northern anticlinal zone
Regional fault
Baicheng Sag
-5000
-6000
-4000
-6500
-3000
Dawanqi field
Qiutalike anticlinal zone
42°
41.5°
81°
N

Figure 2.


Sampling Tubes
Ground Surface
0.3 m
0.6 m
0.9 m
1.2 m
1.5 m
1.8 m
2.1 m
2.4 m
2.7 m
3.0 m
3.5 m
Gas Sampling Tube
4.0 m
a
b

Figure 3.


a
b

Figure 4.


N
41.6°
81.3°
100 m

Figure 5.

CH4 (ppmv)
0
500
1000
1500
2000
2500
3000
0
7000
14000
21000
28000
35000
Depth (m)
0
1
2
3
4
553-9
554-11
554-14
555-16
541-15
546-20
18-7
545-12
546-12
545-13
control area
a
δ13C-CH4（‰）
-50
-45
-40
-35
-30
-25
-20
-15
553-9
554-11
541-15
546-20
545-12
545-13
b

Figure 6.

C_1/C_{2+}
-10
0
10
20
30
40
50
60
70
0
100
200
300
400
500
0
1
2
3
4
Depth (m)
553-9
554-11
554-14
555-16
541-15
546-20
18-7
545-12
546-12
545-13

Figure 7.

CO2 (ppmv)
0
1500
3000
4500
6000
7500
9000
10500
Depth (m)
0
1
2
3
4
553-9
554-11
541-15
546-20
545-12
545-13
control area
a
δ13C-CO2（‰）
-24
-22
-20
-18
-16
-14
-12
-10
-8
Depth (m)
553-9
554-11
541-15
546-20
545-12
545-13
control area
b

Figure 8.

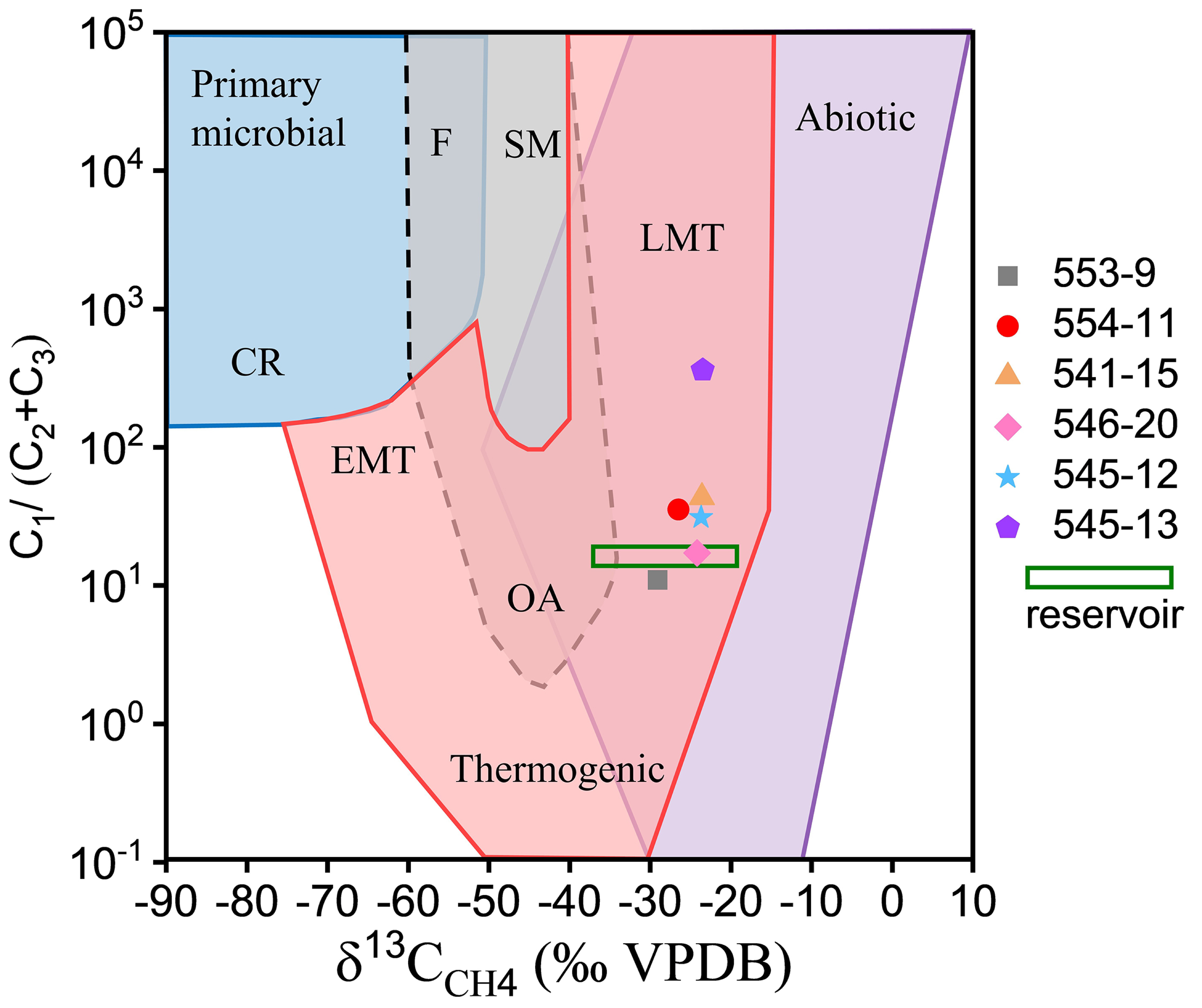

Primary microbial
CR
F
SM
LMT
EMT
OA
Thermogenic
Abiotic
553-9
554-11
541-15
546-20
545-12
545-13
reservoir
$C_1/(C_2+C_3)$
$\delta^{13}C_{CH4}$ (‰ VPDB)
-90
-80
-70
-60
-50
-40
-30
-20
-10
0
10
10^{-1}
10^0
10^1
10^2
10^3
10^4
10^5

Figure 9.

Aug-2014
Jan-2015
Aug-2019
CH4 flux (mg m-2 d-1)
350
300
250
200
150
100
50
5
4
3
2
1
0
-1
552-4
552-5
552-6
553-7
553-8
553-9
553-10
554-11
554-14
554-15
554-18
555-12
555-13
555-16
555-17
555-18
555-19
555-20
555-21
555-22
Measurement points transect MT1

Figure 10.

Aug-2014
Jan-2015
Aug-2019
250
200
150
100
50
5
4
3
2
1
0
-1
CH4 flux (mg m-2 d-1)
541-5
541-6
541-7
541-8
541-9
541-11
541-14
541-15
542-12
542-13
542-26
543-16
543-25
543-28-1
543-28-2
543-28-3
543-28-4
543-28-5
544-16
544-17
544-18
544-23
545-13-1
545-13-2
545-20
545-21
546-19
546-20
Measurement points transect MT2

Figure 11.


Aug-2014
Jan-2015
Aug-2019
150
100
50
5
4
3
2
1
0
-1
CH4 flux (mg m-2 d-1)
13-7
14-6
15-6
16-6
17-5
18-7
19-4
312-10
314-9
316-8
318-7
319-7
324-7
322-6
541-14
542-
543-13
545-12
545-13
546-12
546-13
547-11
549-11
550-10
551-10
552-10
553-9
554-9
556-10
557-8
557-9
558-8
559-7
559-8
561-4
Measurement points transect MT3

Figure 12.

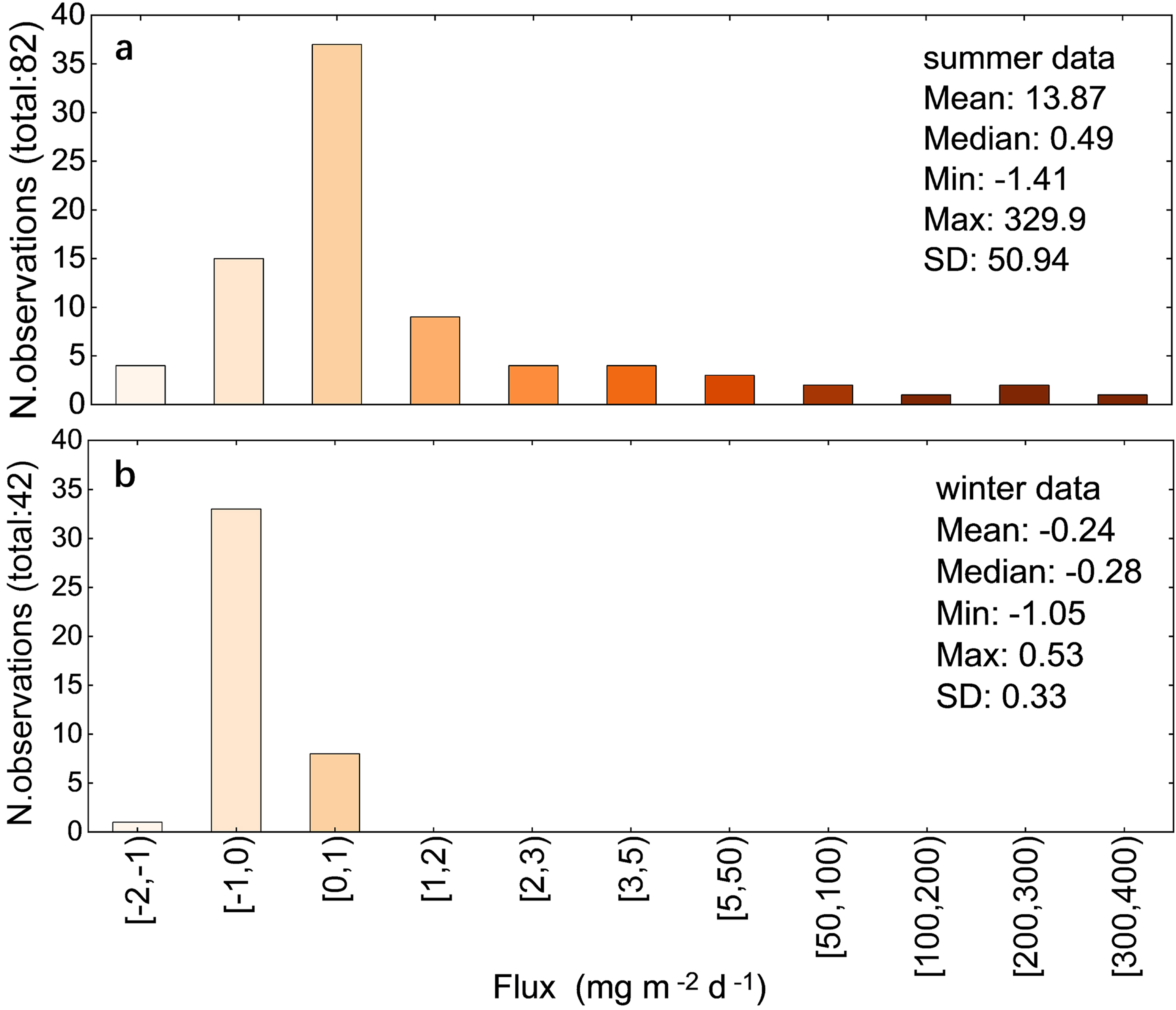
a
summer data
Mean: 13.87
Median: 0.49
Min: -1.41
Max: 329.9
SD: 50.94
N.observations (total:82)
b
winter data
Mean: -0.24
Median: -0.28
Min: -1.05
Max: 0.53
SD: 0.33
N.observations (total:42)
0
5
10
15
20
25
30
35
40
[-2,-1)
[-1,0)
[0,1)
[1,2)
[2,3)
[3,5)
[5,50)
[50,100)
[100,200)
[200,300)
[300,400)
Flux (mg m -2 d -1)